J. Fluid Mech. (1964), *vol.* 20, *part* 4, *pp.* 593–623
Printed in Great Britain

Second-order boundary-layer effects in hypersonic flow past axisymmetric blunt bodies

By R. T. DAVIS† AND I. FLÜGGE-LOTZ
Division of Engineering Mechanics, Stanford University, Stanford, California

(Received 25 May 1964)

First- and second-order boundary-layer theory are examined in detail for some specific flow cases of practical interest. These cases are for flows over blunt axisymmetric bodies in hypersonic high-altitude (or low density) flow where second-order boundary-layer quantities may become important. These cases consist of flow over a hyperboloid and a paraboloid both with free-stream Mach number infinity and flow over a sphere at free-stream Mach number 10. The method employed in finding the solutions is an implicit finite-difference scheme. It is found to exhibit both stability and accuracy in the examples computed. The method consists of starting near the stagnation-point of a blunt body and marching downstream along the body surface. Several interesting properties of the boundary layer are pointed out, such as the nature of some second-order boundary-layer quantities far downstream in the flow past a sphere and the effect of strong vorticity interaction on the second-order boundary layer in the flow past a hyperboloid. In several of the flow cases, results are compared with other theories and experiments.

1. Introduction

The problem of low-density high-speed flow over blunt bodies has attracted wide attention with many methods of attack being developed. The problem is a practical one in that a space vehicle entering the Earth's atmosphere encounters a wide range of flow conditions ranging from free molecular flow at very high altitudes to continuum flow at low altitudes. The intermediate or transition régime between free molecular and compressible viscous continuum flow has been subdivided into various flow régimes depending on the degree of rarefaction. Probstein (1961) and Cheng (1963) discuss these various régimes and methods of attack valid within each régime.

We will be concerned here with penetration into the transition régime from the continuum end, and furthermore we will concern ourselves only with axisymmetric blunt body shapes. In doing this, we employ the compressible Navier–Stokes equations modified with appropriate slip and temperature-jump boundary conditions at the body surface. We could then attempt to solve these complete Navier–Stokes equations or a simplification to them, as has been done by Cheng (1963); however, we will choose an alternate method of approach developed by

† Now with the Engineering Mechanics Department, Virginia Polytechnic Institute.

Van Dyke (1962*a*). This involves solving first- and second-order boundary-layer equations which are found from the Navier–Stokes equations by an expansion in inverse powers of the square root of a Reynolds number. The expansion procedure used is the method of inner and outer expansions and results in replacing the Navier–Stokes equations by two separate sets of equations, one set which is valid in an outer inviscid region, and another set which is valid in an inner viscous (boundary-layer) region. We are interested in the régimes where this expansion parameter is small but not so small that second-order terms in the parameter are negligible. For example, some conditions which would produce the type of flow conditions which we are interested in occur at an altitude of 300,000 ft. at a free-stream Mach number of 5·0. Considering a body of nose radius of 1 ft. under these conditions produces a value of the perturbation parameter of about 0·2. This value will produce considerable deviation in the flow-field quantities from those obtained from the first-order boundary-layer equations. Lenard (1962) has made extensive calculations based on atmospheric conditions and has indicated graphically where these second-order effects become important.

By using a perturbation procedure (such as the one by Van Dyke 1962*a*), the resulting second-order boundary-layer equations are linear and can be subdivided to exhibit several second-order boundary-layer effects. These effects are due to vorticity, longitudinal curvature, transverse curvature, displacement, slip, and temperature jump.

Several authors in addition to Van Dyke (1962*a*) have derived the second-order boundary-layer equations and have provided solutions which are valid in the stagnation-point region only. Among these authors are Lenard (1962) and Maslen (1962). The solutions found by them are obtained as the first term of a Blasius series expansion in the co-ordinate along the body surface. In general these authors are in agreement in their results with the exception of the solutions for the effect of vorticity interaction. This conflict appears now to be resolved with most authors being in agreement as to the correct way to compute this effect.

In this paper the second-order boundary-layer equations as derived by Van Dyke are used and solutions are obtained to these equations by using an implicit finite-difference method. The finite-difference solutions are computed for several nose radii downstream and provide for the first time solutions which are not limited to the stagnation-point region.

Three inviscid flow cases are considered for use with the finite-difference method. These cases are a paraboloid at free-stream Mach number infinity, a hyperboloid at free-stream Mach number infinity, and a sphere at free-stream Mach number 10.† These inviscid solutions used for obtaining the surface-pressure distributions for the boundary-layer computations are exact in the sense that they are numerical solutions to the complete inviscid equations. All of the second-order boundary-layer effects are considered, so that the finite-difference solutions obtained to the boundary-layer equations represent a complete first- and second-order theory.

† Thanks are due to Mr Harvard Lomax and the Ames Research Center of NASA for providing the inviscid solutions for these cases.

The finite-difference method used is an implicit one similar to the method of Flügge-Lotz & Blottner (1962) but altered to improve the accuracy. It is found to be both stable and accurate. Several checks have been made on its accuracy, and it has been found that the error is less than 1 % for most of the examples computed. These examples considered contain solutions to the cases of wall to stagnation-point temperature ratios of 0·2 and 0·6. The case of variable wall temperature could, however, be considered just as easily as these cases of constant wall temperature.

The finite-difference solutions agree with the stagnation-point solutions obtained by a Blasius series expansion near the stagnation-point, however, as the finite-difference solution proceeds away from the stagnation-point, it is found as expected that the solutions obtained differ from the results obtained from using the series results. This is due to the limited range of applicability of one term of the Blasius series expansion.

Some interesting results are found in some of the specific flow cases. One of these is the case of flow past a sphere at free-stream Mach number 10. They show that with diminishing favourable pressure gradient some of the second-order boundary-layer quantities become large when compared with first-order quantities. (For example, v_2, the second-order normal velocity component, becomes large compared to the first-order component v_1.) This indicates that the boundary-layer expansion is not uniformly valid near separation, a fact which has long been known but never before exhibited in this manner. Another interesting case is that of the flow past a hyperboloid at free-stream Mach number infinity. This case exhibits, as expected, the growth of the effect of vorticity interaction as the computations proceed downstream. This indicates that the effect of vorticity interaction will become a first-order effect at distances far downstream from the nose of a hyperboloid.

2. Formulation of the problem

2.1. *Co-ordinate system*

A body of revolution with longitudinal curvature κ^* and nose radius of curvature a^* lies in a flow field with constant velocity U_∞^* (parallel to the body axis) at infinity. The density ρ_∞^* and temperature T_∞^* are given. The specific heat c_p^* and Prandtl number σ are assumed to be constant, and the gas is assumed to be perfect. The co-ordinates of a point in the flow field and the velocity components are described in figure 1. The s^* and n^* co-ordinates are along and normal to the body surface respectively. The u^* and v^* velocity components are parallel to the co-ordinate lines, as shown in figure 1.

2.2. *Dimensionless quantities*

In the following the unstarred quantities are dimensionless and the starred quantities dimensional. For convenience in comparing with Van Dyke (1962*a*) the notation and dimensionless system will parallel his closely. The non-dimensional variables and constants remain bounded in the stagnation region as M_∞

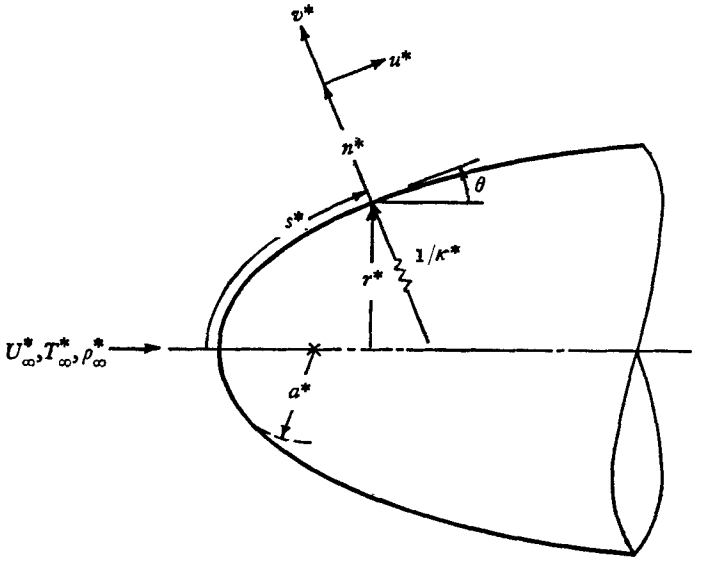

FIGURE 1. Co-ordinate system.

goes to infinity. Co-ordinates and velocity components are explained in figure 1. The quantity j equals 0 for plane flow and equals 1 for axisymmetric flow. Thus

$$s = s^*/a^*, \quad \text{the co-ordinate along body surface,} \tag{2.1a}$$

$$n = n^*/a^*, \quad \text{the co-ordinate normal to body surface,} \tag{2.1b}$$

$$a = a^*/a^* = 1, \quad \text{the nose radius,} \tag{2.1c}$$

$$r = r^*/a^*, \quad \text{the radius to the body surface from the axis of symmetry,} \tag{2.1d}$$

$$u = u^*/U^*_\infty, \quad \text{the velocity component parallel to the body surface,} \tag{2.1e}$$

$$v = v^*/U^*_\infty, \quad \text{the velocity component normal to the body surface,} \tag{2.1f}$$

$$p = p^*/\rho^*_\infty U^{*2}_\infty, \quad \text{the pressure,} \tag{2.1g}$$

$$\rho = \rho^*/\rho^*_\infty, \quad \text{the density,} \tag{2.1h}$$

$$T = T^* c^*_p/U^{*2}_\infty, \quad \text{the absolute temperature,} \tag{2.1i}$$

$$\psi = \psi^*/\rho^*_\infty U^*_\infty a^{*1+j}, \quad \text{the stream function,} \tag{2.1j}$$

$$S = S^*/c^*_p, \quad \text{the entropy,} \tag{2.1k}$$

$$h = h^*/U^{*2}_\infty, \quad \text{the enthalpy,} \tag{2.1l}$$

$$\mu = \mu^*(T^*)/\mu^*(U^{*2}_\infty/c^*_p), \quad \text{the viscosity coefficient,} \tag{2.1m}$$

$$\kappa = \kappa^*/a^*, \quad \text{the longitudinal surface curvature,} \tag{2.1n}$$

$$\bar{\tau} = \bar{\tau}^*/\rho^*_\infty U^{*2}_\infty, \quad \text{the shear stress,} \tag{2.1o}$$

$$q = q^*/\rho^*_\infty U^{*3}_\infty, \quad \text{heat transfer,} \tag{2.1p}$$

$$\bar{\delta}^* = \delta^*/a^*\epsilon, \quad \text{the displacement thickness,} \tag{2.1q}$$

$$C = C^*/T^*_\infty[1 + \tfrac{1}{2}(\gamma - 1) M^2_\infty], \quad \text{the Sutherland constant,} \tag{2.1r}$$

$$R_\infty = U^*_\infty a^* \rho^*_\infty/\mu^*(T^*_\infty), \quad \text{the Reynolds number,} \tag{2.1s}$$

$$\epsilon = [\mu^*(U^{*2}_\infty/c^*_p)/\rho^*_\infty U^*_\infty a^*]^{\frac{1}{2}}, \quad \text{perturbation parameter.} \tag{2.1t}$$

Hereafter all unstarred quantities will be considered to be dimensionless.

2.3. *Reduction of the Navier–Stokes equations to include only second-order terms in a parameter related to a Reynolds number*

The compressible Navier–Stokes equations can be written in the curvilinear co-ordinate system of § 2.1. This has been done, for instance, by Van Dyke (1962*a*) and Maslen (1962). We can then examine these equations keeping in mind that we wish to keep terms of second order in both the boundary layer and outer flow regions (see § 2.4). Using Van Dyke's (1962*a*) equations (2.3)–(2.7), we obtain the following dimensionless equations.

continuity:
$$[(r+n\cos\theta)^j \rho u]_s + [(1+\kappa n)(r+n\cos\theta)^j \rho v]_n = 0; \tag{2.2a}$$

s-momentum:
$$\rho\{uu_s/(1+\kappa n) + vu_n + \kappa uv/(1+\kappa n)\} + p_s/(1+\kappa n) = \epsilon^2[(\mu u_n)_n - \kappa u\mu_n + \mu(\kappa + j\cos\theta/r)\, u_n]; \tag{2.2b}$$

n-momentum:
$$\rho\{uv_s/(1+\kappa n) + vv_n - \kappa u^2/(1+\kappa n)\} + p_n = 0; \tag{2.2c}$$

energy:
$$\rho\{uT_s/(1+\kappa n) + vT_n\} - \{up_s/(1+\kappa n) + vp_n\} = \epsilon^2[\sigma^{-1}(\mu T_n)_n + \sigma^{-1}(\kappa + j\cos\theta/r)\,\mu T_n + \mu u_n^2 - 2\mu\kappa u u_n]; \tag{2.2d}$$

state:
$$p = (\gamma-1)\rho T/\gamma. \tag{2.2e}$$

Four of the above equations are quasi-linear partial differential equations. Two of these partial differential equations are second order and the remaining two are first order. The last equation (state equation) is an algebraic equation. These five equations contain six unknowns (u, v, p, ρ, T and μ) and therefore one more equation is needed in order that a solution can be obtained. This equation is given by a viscosity law which expresses μ, the viscosity, as an algebraic function of the temperature T. The relation which will be used for the viscosity law will be given later.

Comparing these equations (2.2*a–e*) with Van Dyke's (1962*a*) equations (2.3–2.7), we see that we have retained terms to order ϵ in both the outer (i.e. $u = \bar{u}$, $v = \bar{v}$, $n = \bar{n}$, etc.)† and the inner (i.e. $u = \bar{u}$, $v = \epsilon\bar{v}$, $n = \epsilon\bar{n}$, etc.) regions (see § 2.4). These equations are therefore uniformly valid to order ϵ in the entire flow field. This is an especially reasonable reduction when it is borne in mind that the Navier–Stokes equations (without higher-order correction terms) themselves are only physically accurate to the order of the terms retained in the equations (2.2*a–e*) above.

In using equations (2.2*a–e*), we use the Rankine–Hugoniot shock relations as one set of boundary conditions since the effect of shock wave thickness and structure does not appear to the order of the approximation used here. In a higher-order approximation we would, however, have to consider the shock wave structure as well as other higher-order effects which would appear in that approximation, which are not included even in the Navier–Stokes equations. This would require the use of the Burnett equations (whose validity is question-

† Barred quantities indicate quantities which are of order unity in the region of interest.

able) or some other equivalent system of equations. (See Chapman & Cowling 1961, ch. 15, for the higher-order or Burnett correction terms to the Navier–Stokes equations.)

In addition to the Rankine–Hugoniot shock relations to be applied at the shock we must apply the following boundary conditions at the body surface (see Van Dyke 1962*a*, and Street 1960):

$$\left.\begin{aligned} u &= \frac{\epsilon^2 a_1}{p_b}\left[\left(\frac{\gamma-1}{\gamma}\right)T_b\right]^{\frac{1}{2}}\mu u_n \qquad (2.3a)\\ T &= T_b+\frac{\epsilon^2 c_1}{p_b}\left[\left(\frac{\gamma-1}{\gamma}\right)T_b\right]^{\frac{1}{2}}\mu T_n \qquad (2.3b)\end{aligned}\right\} \quad \text{at} \quad n=0.$$

In the above a_1 and c_1 are constants (see Street 1960) and the subscript b refers to the body surface. Equation (2.3*b*) may be replaced by a condition on the wall heat transfer. These boundary conditions allowing for slip and temperature jump at the surface are accurate to the same order as the governing equations (2.2*a–e*).

It is interesting to inquire into the type of the partial differential equations (2.2*a–e*) (i.e. whether they are elliptic, parabolic, or hyperbolic). This is done by studying the characteristics of that system of equations.† There are two possible solutions for the characteristics. Letting β be a curve parameter defining the characteristics, we find for the characteristics one solution,

$$\{ds(\beta)/d\beta\}^2 = 0 \quad \text{or} \quad s = \text{const.}, \qquad (2.4a)$$

and another solution,

$$\frac{dn}{ds} = \left[\frac{v}{u} \pm \frac{1}{u}\left(\frac{p}{\rho}\right)^{\frac{1}{2}}\right](1+\kappa n). \qquad (2.4b)$$

The first solution (2.4*a*) indicates that the equations (2.2*a–e*) are parabolic, whereas the second solution (2.4*b*) indicates that they are hyperbolic. This conclusion is puzzling at first until we notice that the highest derivatives in v and p appear in the n momentum equation (2.2*c*) and the continuity equation (2.2*a*) while the highest derivatives of u and T do not. This means that these two equations (2.2*a* and 2.2*c*) alone determine the nature of the solution for v and p, which happens to be hyperbolic. The other two equations (the s momentum (2.2*b*) and energy (2.2*d*) equations) then behave in a parabolic manner.

This dual nature of the system of equations (2.2*a–e*) may make numerical solution of the complete equations difficult even though parabolic and hyperbolic equations are in principle the easiest to handle by numerical methods. The development of a numerical scheme which handles two of the equations in a manner applicable to parabolic equations while handling the other two as hyperbolic equations may lead to computational difficulties.

Cheng (1963) has derived a similar set of equations which however contain in addition the thin shock layer approximation. His equations (5.1) are similar in form to our equations (2.2*a–e*). It should be noted, however, that Cheng has not included all of the second-order terms. In particular his s-momentum equation and his energy equation have several of the second-order longitudinal and

† For a discussion of the determination of the characteristics of a system of non-linear partial differential equations see Petrovsky (1954, p. 26).

transverse curvature terms missing. We should keep this in mind later when we compare the second-order results obtained from a perturbation analysis with the results of Cheng. (Cheng is aware of the deletion of these terms and has noted that they are omitted in his paper.)

In additon Cheng keeps a term in the n-momentum equation in $(\mu v_n)_n$, which is strictly a third-order term, while other third-order terms are deleted. It is interesting to note that keeping this and other third-order terms in just the n-momentum equation makes the set of equations (2.2*b–d*) parabolic. From a viewpoint of solving the equations (2.2*a–e*) numerically it may be desirable to keep the third-order terms in the n-momentum equation, even though it is inconsistent from an order of magnitude viewpoint.

An examination of equations (2.2*a–e*) shows that the second-order curvature terms have no effect on the parabolic or hyperbolic nature of the differential equations since they involve only lower-order derivatives. It therefore appears that Cheng (1963) could include these terms in his equations (5.1) without increasing the difficulty of solving his equations numerically since his equations would still remain parabolic. This will not be the case if we go to third-order terms in the s-momentum equation (2.2*b*) and in the energy equation (2.2*d*). Appearing in the s-momentum equation will be terms involving u_{ss}, etc., and we will therefore probably return to the original elliptic nature of the Navier–Stokes equations. (This point has not been checked, however.)

We conclude therefore that if one wishes to handle the entire set of equations (2.2*a–e*) at once numerically, it appears that the simplest method of approach would be to treat them in a manner in which the equations are parabolic. This is accomplished as has been noted above by keeping third-order terms in the n-momentum equation while keeping only second-order terms in the other equations. It appears that an approach which treats the entire shock layer at once using parabolic type equations is therefore possible and would be worth looking into.

2.4. *Perturbation method for solution of the problem*

Van Dyke (1962*a*) derived the first- and second-order boundary-layer equations for a plane or axisymmetrical blunt body at zero angle of attack by using the systematic method of inner and outer expansions (or matched asymptotic expansions) due to Lagerstrom, Kaplun and Cole. In deriving the equations he started from the full compressible Navier–Stokes and energy equations, however this is not necessary and equations (2.2*a–e*) could be used since they contain all of the necessary second-order terms. He has found that there are seven second-order effects, one of which is an effect due to an enthalpy gradient across streamlines. In flows where the enthalpy is constant throughout the flow field in front of the shock wave, it will remain constant across the shock wave and therefore the enthalpy gradient will be zero. This is the usual case, and we will therefore not consider this effect. The six remaining second-order boundary-layer effects (whose division is somewhat arbitrary) are entropy gradient (vorticity), transverse curvature, longitudinal curvature, displacement, slip, and temperature jump. We will consider all of these second-order effects; however, we will lump the slip and temperature jump terms together and treat them as one.

(*a*) *Perturbation scheme.* Van Dyke (1962*a*) took the following expansion scheme with the perturbation parameter

$$\epsilon = [\mu^*(U_\infty^{*2}/c_p^*)/\rho_\infty^* U_\infty^* a^*]^{\frac{1}{2}}.$$

This scheme seems reasonable as long as the body is analytic. We could have first left the dependence on ϵ unspecified in the expansion, and upon substitution into the full Navier–Stokes and energy equations we would have found that, when we consider the boundary conditions, the only meaningful expansion scheme is the one given below.

Outer expansion:

$$u(s,n;\epsilon) \sim U_1(s,n)+\epsilon U_2(s,n)+\ldots,\dagger \tag{2.5a}$$
$$v(s,n;\epsilon) \sim V_1(s,n)+\epsilon V_2(s,n)+\ldots, \tag{2.5b}$$
$$p(s,n;\epsilon) \sim P_1(s,n)+\epsilon P_2(s,n)+\ldots, \tag{2.5c}$$
$$\rho(s,n;\epsilon) \sim R_1(s,n)+\epsilon R_2(s,n)+\ldots, \tag{2.5d}$$
$$T(s,n;\epsilon) \sim T_1(s,n)+\epsilon T_2(s,n)+\ldots, \tag{2.5e}$$
$$\psi(s,n;\epsilon) \sim \Psi_1(s,n)+\epsilon\Psi_2(s,n)+\ldots. \tag{2.5f}$$

Inner expansion:

$$u(s,n;\epsilon) \sim u_1(s,N)+\epsilon u_2(s,N)+\ldots, \tag{2.6a}$$
$$v(s,n;\epsilon) \sim \epsilon v_1(s,N)+\epsilon^2 v_2(s,N)+\ldots, \tag{2.6b}$$
$$p(s,n;\epsilon) \sim p_1(s,N)+\epsilon p_2(s,N)+\ldots, \tag{2.6c}$$
$$\rho(s,n;\epsilon) \sim \rho_1(s,N)+\epsilon\rho_2(s,N)+\ldots, \tag{2.6d}$$
$$T(s,n;\epsilon) \sim t_1(s,N)+\epsilon t_2(s,N)+\ldots, \tag{2.6e}$$
$$\psi(s,n;\epsilon) \sim \epsilon\psi_1(s,N)+\epsilon^2\psi_2(s,N)+\ldots. \tag{2.6f}$$

In the above expressions the normal co-ordinates are related by

$$N = n/\epsilon. \tag{2.7}$$

It is also necessary to expand the viscosity in a Taylor series expansion about t_1 as follows:

$$\mu(T) = \mu(t_1)+\epsilon\mu'(t_1)\,t_2+\ldots \tag{2.8}$$

with

$$\mu'(t_1) = (\partial\mu/\partial t)\,t_1. \tag{2.9}$$

The expansion schemes used herein (equations (2.5)–(2.9)) seem reasonable since the boundary-layer thickness at high Mach numbers can be shown to be $O(\epsilon)$, whereas the thickness of the bow shock wave is $O(\epsilon^2)$ and the shock-layer thickness itself is $O(1)$. (See Van Dyke 1962*a*.)

If it is assumed that the viscosity coefficient μ is proportional to T to some power ω, then ϵ, the perturbation parameter, can be written as follows:

$$\epsilon = [(\gamma-1)\,M_\infty^2]^{\omega/2}/R_\infty^{\frac{1}{2}}. \tag{2.10}$$

Here M_∞ is the free-stream Mach number, and R_∞ the Reynolds number formed with the nose radius as reference length.

In all of the work contained in this paper the definition of ϵ used will be that of equation (2.10) and ω will be taken to be $\frac{1}{2}$. This simplification is not necessary and a more exact viscosity law such as Sutherland's could be used; however for

† The symbol $\sim$ means asymptotically equal to.

the flow cases considered herein the value of $\omega = \frac{1}{2}$ gives a good approximation to the Sutherland law for high free-stream Mach numbers.

(*b*) *Matching conditions.* The inner expansion is valid in a reign of $O(\epsilon)$ near the body and the outer expansion is valid in the region outside this region of $O(\epsilon)$. Substituting the inner and outer expansions into the reduced Navier–Stokes and energy equations (2.2*a–e*), we obtain partial differential equations from taking successive terms in ϵ which are of lower order than the original equations. This means that we cannot in general expect the resulting equations to satisfy all of the boundary conditions which the reduced Navier–Stokes and energy equations (2.2*a–e*) satisfied. For instance, we do not expect the outer expansion to satisfy the condition of zero u component of velocity at the wall, or if slip is permitted, the slip condition will be violated. This means that the 'lost' boundary conditions must be replaced by something which makes the problem determinate. These conditions are found to be the matching principle of Lagerstrom (1957). A good explanation of the matching principle along with a more rigorous discussion of inner and outer expansions in general can also be found in a paper by Erdelyi (1961).

The matching principle can be stated as follows:

m-term inner expansion of (p-term outer expansion)
$= p$-term outer expansion of (m-term inner expansion).

Van Dyke (1962*a*) applied this principle with $m = p$ and $m = p - 1$ and obtained the appropriate matching conditions.

(*c*) *First- and second-order equations for the boundary layer.* First the full compressible Navier–Stokes and energy equations are written in the co-ordinate system of § 2.1 non-dimensionalized by equations (2.1*a–t*) (to the second order this produces equations (2.2*a–e*)) and expanded first into the outer expansion and then into the inner expansion by equations (2.5*a–e*) and equations (2.6*a–e*). Then by collecting terms in successive powers of ϵ and equating these to zero, we obtain the partial differential equations describing the outer and inner flows. They comprise both plane and axisymmetric flow. The exponent j equals 0 for plane flow and equals 1 for axisymmetric flow. The subscripts s and N indicate differentiation, and S_1' denotes $dS_1/d\Psi_1$ where S_1 and Ψ_1 are the first-order entropy and stream functions, respectively, in the outer inviscid flow. (The conventional entropy and stream functions obtained from the compressible Euler equations.)

Both the first- and second-order boundary-layer partial differential equations can be shown to be of the parabolic type. This fact will be relied on heavily later when a numerical method of solution applicable to parabolic type equations will be used.

First-order boundary-layer equations

continuity: $$(r^j\rho_1 u_1)_s + (r^j\rho_1 v_1)_N = 0; \tag{2.11}$$

momentum: $$\rho_1(u_1 u_{1s} + v_1 u_{1N}) - (\mu u_{1N})_N = -P_{1s}(s, 0); \tag{2.12}$$

energy: $$\rho_1(u_1 t_{1s} + v_1 t_{1N}) - \mu u_{1N}^2 - (\mu\sigma^{-1} t_{1N})_N = u_1 P_{1s}(s, 0); \tag{2.13}$$

pressure condition:† $$\rho_1 t_1 = (R_1 T_1)_{n=0}; \tag{2.14}$$

† In both the first- and second-order boundary-layer equations the pressure condition replaces the n-momentum equation.

boundary conditions:
$$u_1(s,0) = v_1(s,0) = 0, \tag{2.15a,b}$$
$$t_1(s,0) = T_b(s), \tag{2.15c}$$

or a condition on heat transfer at the wall;

matching conditions:
$$u_1(s,N) \sim U_1(s,0), \quad t_1(s,N) \sim T_1(s,0) \quad \text{as} \quad N \to \infty. \tag{2.16a,b}$$

These are the familiar compressible boundary-layer equations in non-dimensional form, and the number of equations equals the number of unknowns if a viscosity law is specified.

Second-order boundary-layer equations (see Van Dyke 1962*a*, pp. 54–55)

continuity:
$$[r^j(\rho_1 u_2 + \rho_2 u_1)]_s + [r^j(\rho_1 v_2 + \rho_2 v_1)]_N$$
$$= \underset{\text{V.}}{0} - \underset{\text{L.C.}}{\kappa r^j (N\rho_1 v_1)_N} - \underset{\text{T.C.}}{j\left[\left(r^j \frac{\cos\theta}{r} N\rho_1 u_1\right)_s - \left(r^j \frac{\cos\theta}{r} N\rho_1 v_1\right)_N\right]} + \underset{\text{D.}}{0} + \underset{\text{S.+T.J.}}{0}; \tag{2.17}$$

momentum:
$$\rho_1(u_1 u_{2s} + u_2 u_{1s} + v_1 u_{2N} + v_2 u_{1N}) + \rho_2(u_1 u_{1s} + v_1 u_{1N}) - (\mu u_{2N} + \mu' u_{1N} t_2)_N$$
$$= \underset{\text{V.}}{-r^j [R_1^2 T_1 S_1' V_2]_{n=0}} + \underset{\text{L.C.}}{\kappa[N(\mu u_{1N})_N + \mu u_{1N} - \mu' u_1 t_{1N} - N\rho_1 v_1 u_{1N} - \rho_1 u_1 v_1]}$$
$$- \frac{\partial}{\partial s}\kappa(R_1 U_1^2)_{n=0}\left[\underset{\text{L.C.}}{N + \int_N^\infty \left\{1 - \frac{\rho_1 u_1^2}{(R_1 U_1^2)_{n=0}}\right\} dN}\right] + \underset{\text{T.C.}}{j\frac{\cos\theta}{r}\mu u_{1N}}$$
$$+ \underset{\text{D.}}{[R_1(U_1 U_2)_s + R_2 U_1 U_{1s}]_{n=0}} + \underset{\text{S.+T.J.}}{0}; \tag{2.18}$$

energy:
$$\rho_1(u_1 t_{2s} + u_2 t_{1s} + v_1 t_{2N} + v_2 t_{1N}) + \rho_2(u_1 t_{1s} + v_1 t_{1N}) - u_2 P_{1s}(s,0)$$
$$- (\mu\sigma^{-1} t_2)_{NN} - 2\mu u_{1N} u_{2N} - \mu' u_{1N}^2 t_2$$
$$= \underset{\text{V.}}{r^j u_1 [R_1^2 T_1 S_1' V_2]_{n=0}} + \underset{\text{L.C.}}{\kappa[N\rho_1 u_1 t_{1s} + \sigma^{-1}\mu t_{1N} + \rho_1 u_1^2 v_1 - N u_1 P_{1s}(s,0) - 2\mu u_1 u_{1N}]}$$
$$+ u_1 \frac{\partial}{\partial s}\kappa(R_1 U_1^2)_{n=0}\left[\underset{\text{L.C.}}{N + \int_N^\infty \left\{1 - \frac{\rho_1 u_1^2}{(R_1 U_1^2)_{n=0}}\right\} dN}\right]$$
$$+ \underset{\text{T.C.}}{j\sigma^{-1}\frac{\cos\theta}{r}\mu t_{1N}} - \underset{\text{D.}}{u_1[R_1(U_1 U_2)_s + R_2 U_1 U_{1s}]_{n=0}} + \underset{\text{S.+T.J.}}{0}; \tag{2.19}$$

pressure condition:
$$\rho_1 t_2 + \rho_2 t_1 = \underset{\text{V.}}{0} + \frac{\gamma}{\gamma - 1}\kappa(R_1 U_1^2)_{n=0}\left[\underset{\text{L.C.}}{N + \int_N^\infty \left\{1 - \frac{\rho_1 u_1^2}{(R_1 U_1^2)_{n=0}}\right\} dN}\right]$$
$$+ \underset{\text{T.C.}}{0} + \underset{\text{D.}}{(R_1 T_2 + R_2 T_1)_{n=0}} + \underset{\text{S.+T.J.}}{0}; \tag{2.20}$$

boundary conditions:

$$u_2(s,0) = \underset{\text{V.}}{0} + \underset{\text{L.C.}}{0} + \underset{\text{T.C.}}{0} + \underset{\text{D.}}{0} + \underset{\text{S.+T.J.}}{a_1\left[\frac{1}{p_1}\sqrt{\left(\frac{\gamma-1}{\gamma}t_1\right)}\mu u_{1N}\right]_{N=0}}, \tag{2.21a}$$

$$v_2(s,0) = \underset{\text{V.}}{0} + \underset{\text{L.C.}}{0} + \underset{\text{T.C.}}{0} + \underset{\text{D.}}{0} + \underset{\text{S.+T.J.}}{0}, \tag{2.21b}$$

$$t_2(s,0) = \underset{\text{V.}}{0} + \underset{\text{L.C.}}{0} + \underset{\text{T.C.}}{0} + \underset{\text{D.}}{0} + \underset{\text{S.+T.J.}}{c_1\left[\frac{1}{p_1}\sqrt{\left(\frac{\gamma-1}{\gamma}t_1\right)}\mu t_{1N}\right]_{N=0}}, \tag{2.21c}$$

or a condition on the second-order term for heat transfer at the wall;

matching conditions:

$$\left.\begin{aligned} u_2(s,N) &\sim -r^j N[R_1 T_1 S_1']_{n=0} - \kappa N[U_1]_{n=0} + 0 + [U_2]_{n=0} + 0 \\ &\text{V.} \qquad\qquad \text{L.C.} \quad \text{T.C.} \quad \text{D.} \quad \text{S.+T.J.} \end{aligned}\right\} \tag{2.22a}$$

$$\left.\begin{aligned} t_2(s,N) &\sim r^j N[R_1 T_1 S_1' U_1]_{n=0} + \kappa N[U_1^2]_{n=0} + 0 + [T_2]_{n=0} + 0 \\ &\text{V.} \qquad\qquad \text{L.C.} \quad \text{T.C.} \quad \text{D.} \quad \text{S.+T.J.} \end{aligned}\right\} \quad \text{as} \quad N \to \infty, \tag{2.22b}$$

The V., L.C., T.C., D., and S.+T.J. appearing under the right-hand terms in the preceding equations signify the contributions due to vorticity, longitudinal curvature, transverse curvature, displacement, and slip and temperature jump, respectively. Since the equations are linear, these various effects can be solved for separately. This will be done in the numerical examples. This division is somewhat arbitrary and it is possible to divide the second-order effects in other ways. In particular the vorticity and displacement terms have been divided in another way by some authors. The way that they are divided here is the same as that of Van Dyke (1962*a*) upon whose work this section is based. Van Dyke (1962*b*) has discussed how various authors have divided the second-order terms, and in his terminology the displacement term used herein should be called the 'displacement speed' term.

The quantities with the subscripts one in equations (2.17)–(2.22) are known from the solution of the first-order boundary-layer equations (2.11)–(2.16) and from the first-order inviscid solution. Knowing these quantities, equations (2.17)–(2.22) can be solved if a viscosity law is specified (the number of equations equals the number of unknowns).

The term $S_1'(0)$ appearing in the second-order equations is defined as

$$S_1'(0) = \frac{dS_1(0)}{d\Psi_1} = -\frac{4(\gamma-1)(M_\infty^2-1)^2\alpha^{1+j}0^{1-j}}{[2\gamma M_\infty^2-(\gamma-1)][2+(\gamma-1)M_\infty^2]}, \tag{2.23}$$

where $0^{1-j} = 0$ for plane flow and 1 for axisymmetric flow. α is the ratio of body to shock nose radius. Therefore we see that there is no effect of vorticity for plane flow to the second order.

Appearing on the right-hand side of the second-order momentum equation (2.22) is the quantity $V_2(s,0)$. It can be shown that by using the matching principle, the relation (2.30) for the displacement thickness and the first-order continuity equation (2.11), the following relation exists,

$$V_2(s,0) = \{1/r^j R_1(s,0)\}\, d\{r^j R_1(s,0)\, U_1(s_1,0)\, \bar{\delta}^*\}/ds; \tag{2.24}$$

this shows that the boundary layer through its displacement thickness acts on the outer flow as a distribution of sources along the body surface. This relation (2.24) will be used in the numerical step-by-step computations. Equation (2.24) means that we do not need to solve the second-order problem for the outer flow in order to calculate the second-order effect of vorticity in the boundary layer. As would be expected, the first-order equations for the outer flow do not show a viscosity influence and therefore turn out to be the familiar compressible Euler equations, and the second-order equations for the outer flow show that to the second order in the outer flow the flow field is that about the original body plus displacement thickness.

(*d*) *Heat transfer, shear stress, and displacement thickness.* The non-dimensional heat transfer and shear stress are defined as follows:

heat transfer:

$$q = -\frac{1}{\rho_\infty^* U_\infty^{*3}}\left[\frac{c_p^*}{\sigma}\mu^*\frac{\partial T^*}{\partial n^*} + \mu^* u^*\frac{\partial u^*}{\partial n^*}\right]_{n^*=0} = \epsilon q_1 + \epsilon^2 q_2 + \ldots; \dagger \qquad (2.25)$$

shear stress:

$$\bar{\tau} = \frac{1}{\rho_\infty^* U_\infty^{*2}}\left[\mu^*\frac{\partial u^*}{\partial n^*}\right]_{n^*=0} = \epsilon\bar{\tau}_1 + \epsilon^2\bar{\tau}_2 + \ldots. \qquad (2.26)$$

In terms of the first- and second-order boundary-layer quantities the non-dimensional heat transfer and shear stress are then found to be as follows:

heat transfer:

$$q = -\epsilon\frac{1}{\sigma}\left[\mu\frac{\partial t_1}{\partial N}\right]_{N=0} - \epsilon^2\frac{1}{\sigma}\left[\mu\frac{\partial t_2}{\partial N} + \mu' t_2\frac{\partial t_1}{\partial N} + \sigma\mu u_2\frac{\partial u_1}{\partial N}\right]_{N=0} + \ldots; \qquad (2.27)$$

shear stress:

$$\bar{\tau} = \epsilon[\mu\,\partial u_1/\partial N]_{N=0} + \epsilon^2[\mu\,\partial u_2/\partial N + \mu' t_2\,\partial u_1/\partial N]_{N=0} + \ldots. \qquad (2.28)$$

The displacement thickness for the first-order boundary layer is defined as

$$\delta^* = \int_0^\infty \left(1 - \frac{\rho_1^* u_1^*}{(R_1^* U_1^*)_{n^*=0}}\right) dn^*; \qquad (2.29)$$

using non-dimensional quantities we therefore get

$$\bar{\delta}^* = \int_0^\infty \left(1 - \frac{\rho_1 u_1}{(R_1 U_1)_{n=0}}\right) dN. \qquad (2.30)$$

3. Solutions for hypersonic flow past axisymmetric blunt bodies

3.1. *Problems to be considered*

In this section an implicit finite-difference method will be used for solving some typical first- and second-order boundary-layer problems. In all cases the gas will be assumed to be perfect with ratio of specific heats $\gamma = 1{\cdot}4$, the Prandtl number σ will be assumed a constant equal to 0·7 and the viscosity law will be taken to be the square root law (i.e. $\mu \propto T^{\frac{1}{2}}$). The particular examples chosen are a paraboloid and a hyperboloid at free-stream Mach number infinity and a sphere at free-stream Mach number 10. The solutions for the inviscid flow past these bodies have been provided by H. Lomax of the Ames Research Center of the NASA. They are exact solutions in the sense that the full inviscid Euler equations were

† The second term in the heat transfer expression arises due to slip at the wall, see Maslen (1958).

solved numerically for obtaining them (see Inouye & Lomax 1962 for a description of the method of solution). Such a numerical inviscid solution is sufficient for solving the first-order boundary-layer equations and also for solving for all of the second-order effects with the exception of displacement thickness.

To be exact, the effect of displacement thickness should be solved for by perturbing the numerical solution for the first-order inviscid solution; however, this will not be done and the flow due to displacement thickness will be solved for by approximating the body plus displacement thickness by the original body shifted and expanded to fit the body consisting of old body plus displacement thickness. This should give a good approximation to the flow due to displacement thickness. The fit to the displacement thickness curve by this approximation will be demonstrated to be good in most cases.

Due to the favourable pressure gradient at the surface in both the flow past the paraboloid and the hyperboloid, boundary-layer separation will not occur in either of these cases; however, separation will occur in the case of flow past a sphere. It will be interesting to investigate the flow near separation, and in particular study the behaviour of the second-order terms. It is generally accepted that boundary-layer theory is not valid in the region of separation, and if this is true, we would expect this to show up in the second-order terms as the point of separation is approached. We would expect some of the second-order terms to become large near separation.

3.2. *Solution of the first- and second-order boundary-layer equations by finite-difference methods*

Both the first- and second-order compressible boundary-layer equations, equations (2.11)–(2.16) and (2.17)–(2.22), are systems of parabolic partial differential equations. As far as a numerical solution is concerned, the most important feature of both of these sets of equations is that they are parabolic. This feature allows the equations to be integrated by a step-by-step procedure along the body surface. In order to put the equations in a form in which this step-by-step procedure can be carried out, the derivatives with respect to s must be replaced by finite-difference quotients. We will also assume that the derivatives with respect to N are replaced by difference quotients in order to obtain a set of difference equations rather than the original set of difference-differential equations.

The manner in which the differential quotients in the s-direction are replaced with s-difference quotients will determine whether the resulting difference equations will be of the explicit or implicit type. If forward s-difference quotients are taken, the equations will be of the explicit type, and if backward s-difference quotients are taken, they will be implicit. The number of grid points used in forming the difference quotients in the s-direction will determine the accuracy of the replacement of differentials by differences in that direction. In an implicit method an increase of the number of grid points is usually helpful in obtaining more accurate solutions; however, in an explicit method this will usually decrease the stability of the difference-equation scheme, as compared to that of the simplest two-point forward-difference scheme.

The explicit method of solution has been examined in detail in Crocco variables by Flügge-Lotz & Baxter (1956), and Baxter & Flügge-Lotz (1957). Among other investigations into explicit methods of solution are those of Flügge-Lotz & Yu (1960) and Wu (1960). All of these methods have found only limited application due almost entirely to the severe requirements for stability placed on their difference equations. Explicit methods, such as the Dufort–Frankel scheme used by Raetz (1957), may be used to overcome the stability problem; however, the truncation errors involved in that particular method may lead to inaccuracies which may be above those which can be tolerated, especially when one is considering evaluating second-order boundary-layer quantities. For these reasons the idea of using explicit methods for calculating solutions to the first- and second-order boundary-layer equations will not be considered further, and we will restrict ourselves to the implicit method only.

Until the present the only implicit finite-difference method developed for treating the boundary-layer equations has been that of Flügge-Lotz & Blottner (1962) (excluding a modification of Flügge-Lotz & Blottner's method by Cheng 1963 to treat these thin shock-layer equations). The method Smith & Clutter (1963*a*, *b*) developed somewhat later is actually fairly close in idea to Flügge-Lotz & Blottner's method, even though it cannot strictly be called a finite-difference method since the N-derivatives are left in differential form and not replaced by finite differences. It should be referred to more properly as a mixed or difference-differential method. Both of these methods have been shown to be accurate and to give results in a reasonable computing time.

In order to form a practical implicit-difference scheme, the difference equations must be linearized so that the simultaneous algebraic equations can easily be solved. This may be achieved without a sacrifice in accuracy, as can be borne out in comparison with known analytic results. The method of linearization and solution used closely parallel that of Flügge-Lotz & Blottner (1962) with modifications to improve the accuracy. These modifications primarily involve the use of three-point backward differences in the s-direction to produce truncation errors of order $(\Delta s)^2$ rather than Δs. This is desirable since the errors in the N-direction in their method were of order $(\Delta N)^2$. The advantage of using the three-point difference scheme will be greater accuracy with a slightly larger step size in Δs with very little increase in computing time per step. (The overall computing time may even be reduced due to the larger step size.) Details of the implicit method will be purposely omitted; for those the reader is referred to Flügge-Lotz & Blottzer (1962) and Davis & Flügge-Lotz (1963).

3.3. *Boundary-layer solutions for flow past a paraboloid at free-stream Mach number infinity*

The inviscid surface pressure distribution for this case (provided by H. Lomax) is given in figure 2 as a function of the dimensionless distance s measured along the surface of the body from the stagnation-point. By the method of least squares, polynomials were determined which represent the original numerical pressure data to at least three places at all points along the body surface. This

required the use of two polynomials in the case of a parabola, one which was good near the nose and another which was good further back on the body surface.

(*a*) *First-order solutions for the paraboloid.* Figures 3–5 give the first-order results for the flow past the paraboloid at $M_\infty = \infty$, $\gamma = \frac{7}{5}$. A variety of wall conditions were chosen, including the case of the insulated wall. It may be noted

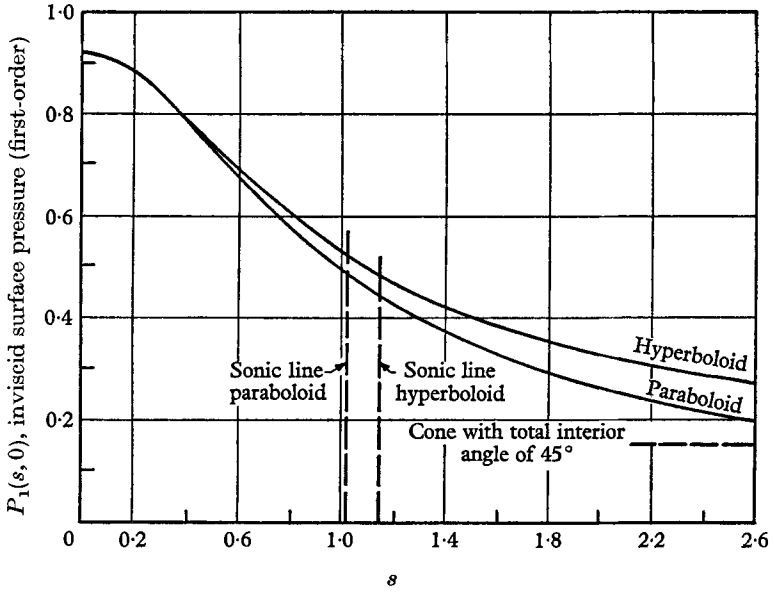

FIGURE 2. Surface-pressure distribution for a paraboloid and a hyperboloid at $M_\infty = \infty$, $\gamma = \frac{7}{5}$.

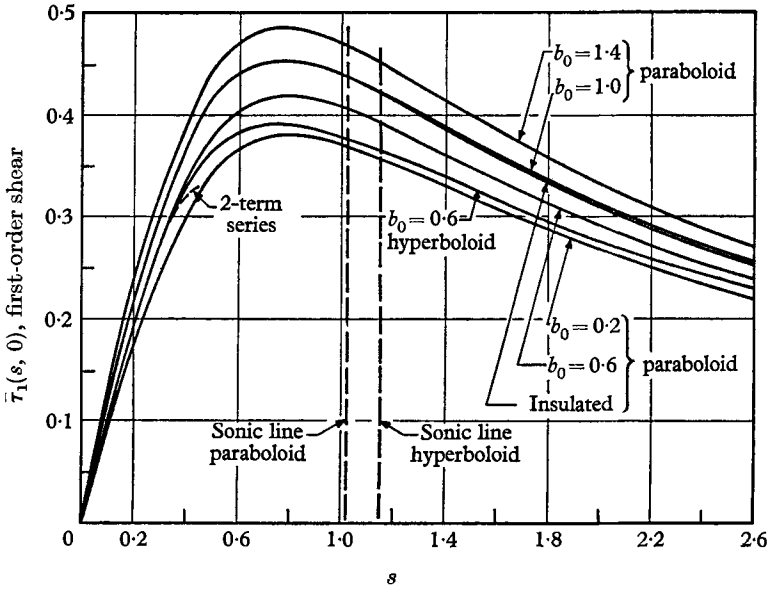

FIGURE 3. First-order shear on a paraboloid and a hyperboloid at $M_\infty = \infty$, $\gamma = \frac{7}{5}$.

that the results for the insulated wall vary only slightly from the results obtained for the case of wall to stagnation-point temperature ratio b_0 of 1·0.

In order to check the accuracy of the finite-difference solution, the results from it are compared with two terms of the Blasius series for the first-order boundary-layer theory (see Davis & Flügge-Lotz 1964). These results are given in table 1 for the case of wall to stagnation-point temperature ratio b_0 of 0·6. We see that at first the series solution and finite-difference solution do not agree well. This is due to the fact that the initial profiles obtained from the Blasius

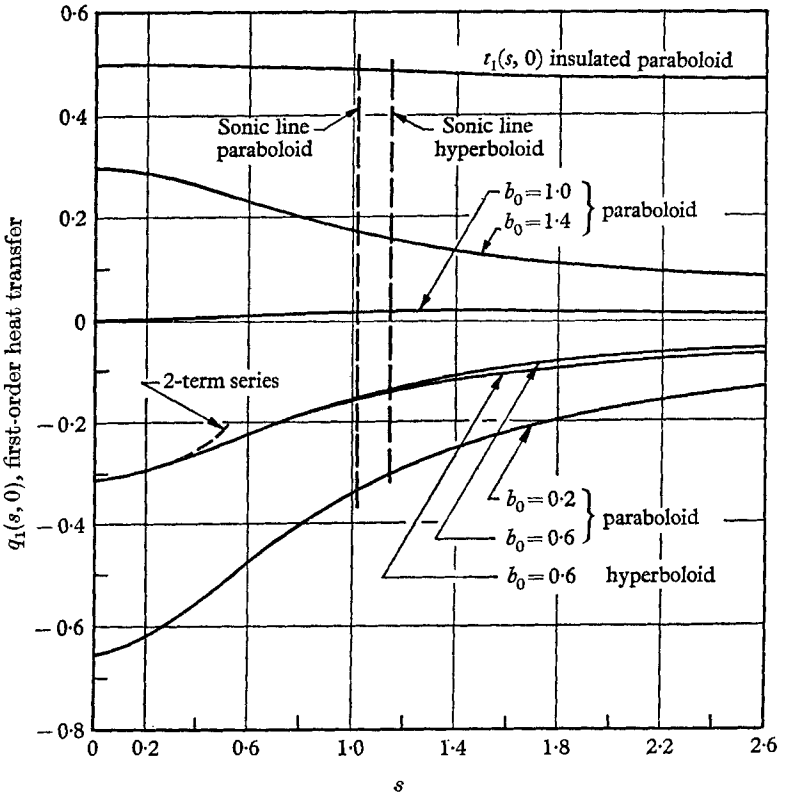

FIGURE 4. First-order heat transfer on a paraboloid and a hyperboloid at $M_\infty = \infty$, $\gamma = \frac{7}{5}$.

	Series results			Finite-difference results		
s	$\bar{\tau}_1(s, 0)$	$q_1(s, 0)$	$\bar{\delta}^*$	$\bar{\tau}_1(s, 0)$	$q_1(s, 0)$	$\bar{\delta}^*$
0·05	0·0524	−0·3091	0·1429	0·0517	−0·2858	0·1387
0·10	0·1036	−0·3063	0·1444	0·1034	−0·3041	0·1441
0·15	0·1524	−0·3017	0·1468	0·1524	−0·3010	0·1469
0·20	0·1977	−0·2953	0·1503	0·1982	−0·2953	0·1504
0·25	0·2383	−0·2870	0·1547	0·2401	−0·2881	0·1549
0·30	0·2729	−0·2769	0·1602	0·2775	−0·2798	0·1603
0·35	0·3005	−0·2650	0·1666	0·3101	−0·2707	0·1667

TABLE 1

series are not exact solutions to the finite-difference equations. This causes the finite-difference solutions to oscillate for a few steps, but then this oscillation dies out and after a few steps (actually about 20, since the results presented here are obtained from computations with $\Delta s = 0{\cdot}005$), the series solution agrees quite well with the finite-difference solution. This agreement is seen to be to three or

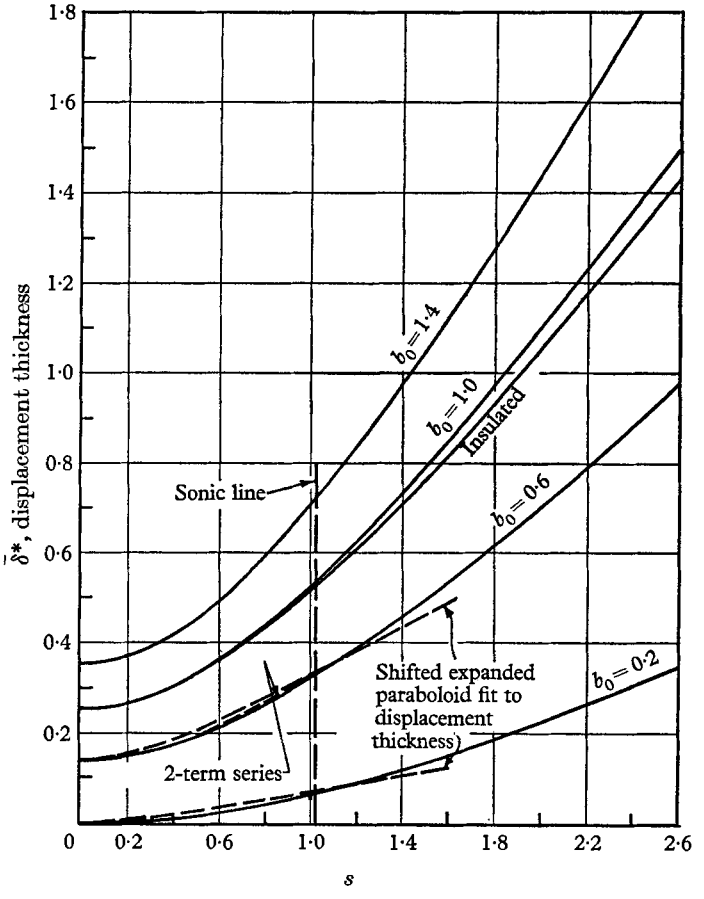

FIGURE 5. Displacement thickness on a paraboloid at $M_\infty = \infty$, $\gamma = \frac{7}{5}$.

four places from $s = 0{\cdot}15$ to $s = 0{\cdot}25$. We then see that the series solution begins to diverge from the finite-difference solution as s increases. This is due to the fact that only two terms of the Blasius series solution were used and hence the range of its validity is limited to a region close to the stagnation-point. In cases where exact solutions are known for the complete boundary-layer equations (for example, the flat plate), it has been found that the accuracy of the finite-difference method increases as the computations proceed downstream. For this reason we expect that we will obtain even better accuracy than has been displayed here as we proceed away from the stagnation-point. The results for two terms of the Blasius series are plotted on figures 3–5 for the case of $b_0 = 0{\cdot}6$ for comparison with the finite-difference solutions.

(*b*) *Second-order solutions for the paraboloid.* The finite-difference solutions to the second-order boundary-layer equations are carried out in exactly the same manner as the first-order equations. Several points which have not yet been covered will, however, be discussed here.

In order to compute the second-order effect of displacement thickness on the boundary layer, it is necessary to compute the outer flow corresponding to a paraboloid thickened by the displacement thickness. The values for the desired second-order quantities, assuming that the body plus displacement thickness can be approximated by a shifted, expanded paraboloid are obtained as follows. If the original body-nose radius of curvature is given by a^* and the body approximating the original body plus displacement thickness has a nose radius of curvature a_1^*, then the (s, n)-co-ordinates are non-dimensionalized by a^* and the (s_1, n_1)-co-ordinates by a_1^*. The (s, n)-co-ordinates correspond to the original body and the (s_1, n_1)-co-ordinates correspond to the shifted expanded body approximating the original body plus displacement thickness. In terms of these quantities we have the following:

$$\epsilon U_2(s,0) = (s_1 - s)\,\partial U_1(s,0)/\partial s - (n_1 - n)\,[\kappa U_1 + r^j R_1 T_1 S_1']_{n=0}, \tag{3.1}$$

$$\epsilon R_2(s,0) = (s_1 - s)\,\partial R_1(s,0)/\partial s + (n_1 - n)\,[\kappa R_1 U_1^2/(\gamma - 1)\,T_1 - r^j R_1^2 U_1 S_1']_{n=0}, \tag{3.2}$$

$$\epsilon T_2(s,0) = (s_1 - s)\,\partial T_1(s,0)/\partial s + (n_1 - n)\,[\kappa U_1^2 + r^j U_1 T_1 S_1']_{n=0}, \tag{3.3}$$

where $s_1 - s$ and $n_1 - n$ are determined approximately so as to give the best fit of the shifted expanded body to the original body plus displacement thickness. In obtaining the above expressions ((3.1)–(3.3)), the quantities $\partial U_1(s,0)/\partial n$, $\partial R_1(s,0)/\partial n$ and $\partial T_1(s,0)/\partial n$ are needed. These can be obtained from Van Dyke (1962*a*, p. 47).

We will also need the relation for $V_2(s,0)$. Expanding to find $V_2(s,0)$, as was done in obtaining $U_2(s,0)$, $R_2(s,0)$ and $T_2(s,0)$ in equations (3.1)–(3.3), we find

$$\epsilon V_2(s,0) = U_1(s,0)\,d(n - n_1)/ds + (s_1 - s)\,\partial V_1(s,0)/\partial s + (n_1 - n)\,\partial V_1(s,0)/\partial n. \tag{3.4}$$

The first term on the right-hand side arises because the velocity components in the (s, n)-co-ordinates are in a slightly different direction from the velocity components in the (s_1, n_1)-direction. This effect is negligible in the expression for $U_2(s,0)$ given by equation (3.1). Using the fact that $\partial V_1(s,0)/\partial s = 0$, we then obtain

$$\epsilon V_2(s,0) = U_1(s,0)\,d(n - n_1)/ds + (n_1 - n)\,\partial V_1(s,0)/\partial n. \tag{3.5}$$

Using the continuity equation to evaluate $\partial V_1(s,0)/\partial n$, we then find that

$$\epsilon V_2(s,0) = -\{1/r^j R_1(s,0)\}\,d[r^j R_1(s,0)\,U_1(s,0)\,(n_1 - n)]/ds. \tag{3.6}$$

Comparing this with equation (2.24), we obtain

$$(n_1 - n) = -\epsilon \bar{\delta}^*. \tag{3.7}$$

Let the shifted, expanded paraboloid be situated with respect to the original paraboloid as indicated in figure 6. Then we find that after some simple but tedious computation

$$(s_1 - s) = -\epsilon r[\zeta_1 + \tfrac{1}{2} r^2(\zeta_1 + \zeta_2)]/(1 + r^2)^{\frac{1}{2}}, \tag{3.8}$$

$$(n_1 - n) = -\epsilon\{\zeta_1 + \zeta_2 - [\zeta_1 + \tfrac{1}{2} r^2(\zeta_1 + \zeta_2)]/(1 + r^2)\}\,(1 + r^2)^{\frac{1}{2}}. \tag{3.9}$$

Since the relation $\epsilon\bar{\delta}^* = -(n_1 - n)$ exists, we determine the constants so that the expression (3.9) gives a good fit to the displacement thickness. Figure 5 includes plots of equation (3.9) which have been fitted to the displacement thickness curves. In general, in the subsonic region the fit is quite good, whereas it may not be so good further back on the body surface.

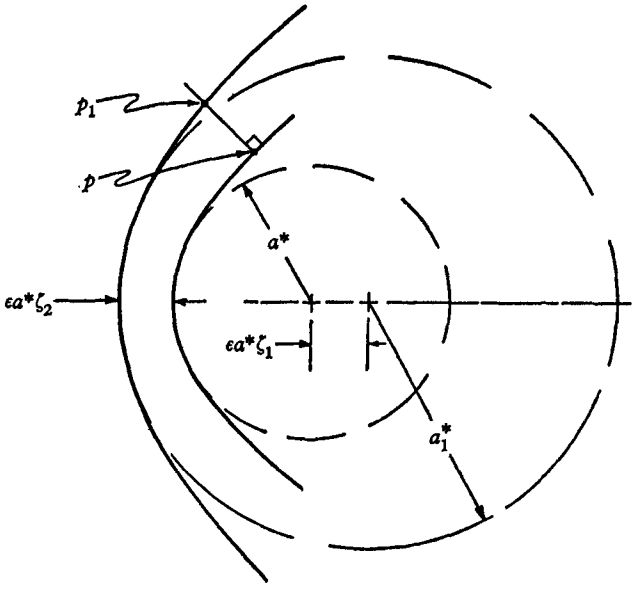

FIGURE 6. Co-ordinate system for a shifted, expanded, paraboloid.

The other second-order outer quantity which is needed for solving the second-order boundary-layer equations is $V_2(s, 0)$. This quantity is given by equation (2.24) and can be computed knowing first-order boundary-layer quantities only.

All of the other quantities appearing in the second-order equations can be handled straightforwardly. The constants a_1 and c_1 appearing in the second-order boundary conditions (2.21) have been taken to be $(\frac{1}{2}\pi)^{\frac{1}{2}}$ and $\frac{15}{8}(\frac{1}{2}\pi)^{\frac{1}{2}}$, respectively.

Figures† 6 and 8 show the second-order results for shear and heat transfer (see equations (2.25)–(2.28)) for a wall to stagnation-point temperature ratio b_0 of 0·6. The curves for the displacement effect are not so accurate as the other curves, because of the approximation involved in using equations (3.1)–(3.3); however, they do give us a good insight into how large this effect of displacement thickness is. In this particular case ($b_0 = 0{\cdot}6$) it is larger than any of the other second-order effects with the exception of vorticity. Figure 7 contains a dashed portion on the curve for the effect of displacement thickness. This indicates that the accuracy in that region is doubtful due to the fact that the approximation to the displacement thickness curve (see figure 5) does not fit so well in that region. Figures 9 and 10 give the results for second-order shear and heat transfer on the same paraboloid, but with a wall to stagnation-point temperature ratio b_0 of 0·2.

† In the figures in this paper, $\bar{\tau}_2$, q_2, etc. (the second-order contributions to shear, heat transfer, etc.) are understood to represent only the contributions due to the particular effect being considered.

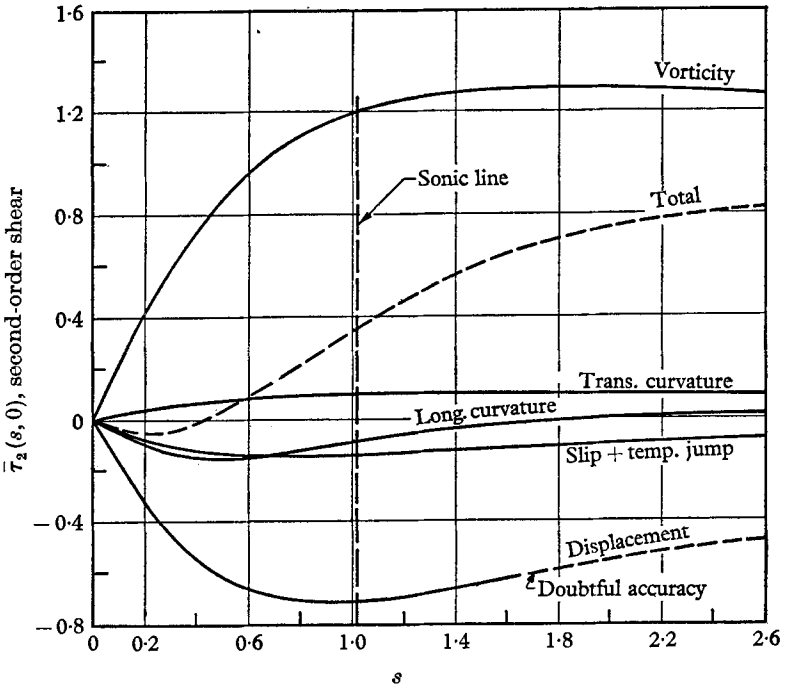

FIGURE 7. Second-order shear on a paraboloid at $M_\infty = \infty$, $\gamma = \frac{7}{5}$, $b_0 = 0{\cdot}6$.

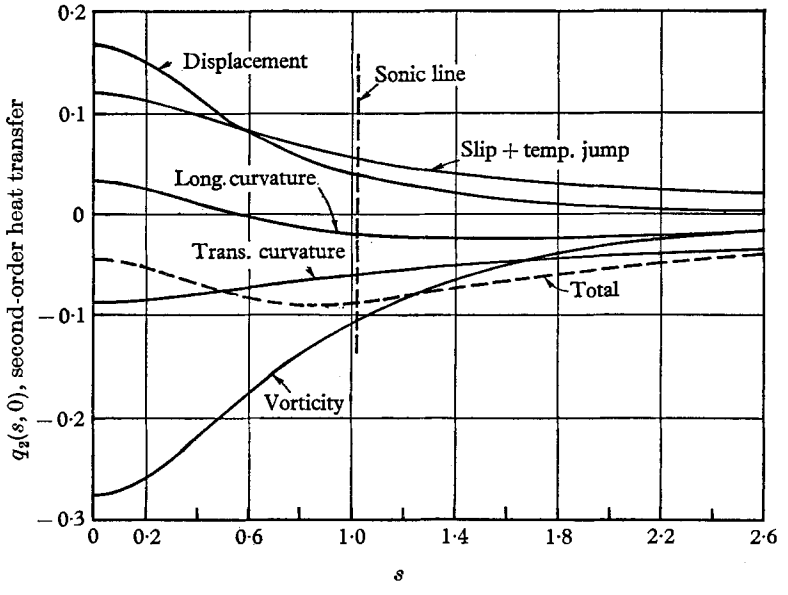

FIGURE 8. Second-order heat transfer on a paraboloid at $M_\infty = \infty$, $\gamma = \frac{7}{5}$ b_0, $= 0{\cdot}6$.

3.4. *Boundary-layer solutions for flow past a hyperboloid at free-stream Mach number infinity*

The pressure distribution for the hyperboloid at free-stream Mach number infinity is given in figure 2. This pressure distribution was also provided by H. Lomax from a numerical solution to the full inviscid equations. The particular

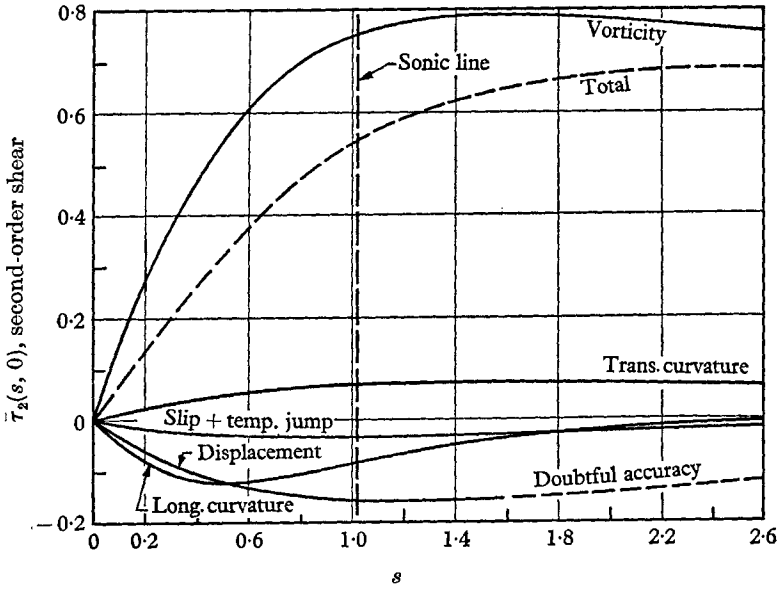

FIGURE 9. Second-order shear on a paraboloid at $M_\infty = \infty$, $\gamma = \frac{7}{5}$, $b_0 = 0{\cdot}2$.

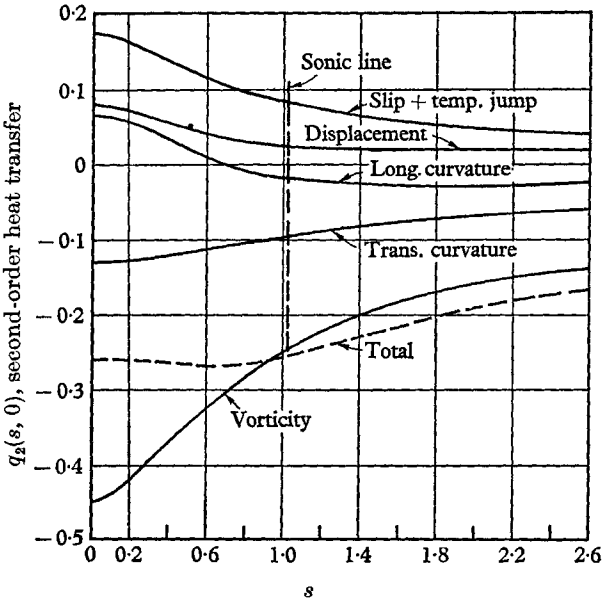

FIGURE 10. Second-order heat transfer on a paraboloid at $M_\infty = \infty$, $\gamma = \frac{7}{5}$, $b_0 = 0{\cdot}2$.

hyperboloid considered is one which is asymptotic to a cone which opens to a total interior angle of 45°. For ease in computation, the numerical data of Lomax were approximated by an analytical curve (method of least squares).

(*a*) *First-order solutions for the hyperboloid.* Figures 3, 4 and 11 show the first-order results for flow over the hyperboloid with a wall to stagnation-point temperature ratio $b_0 = 0{\cdot}6$. Near the stagnation-point these results agree well

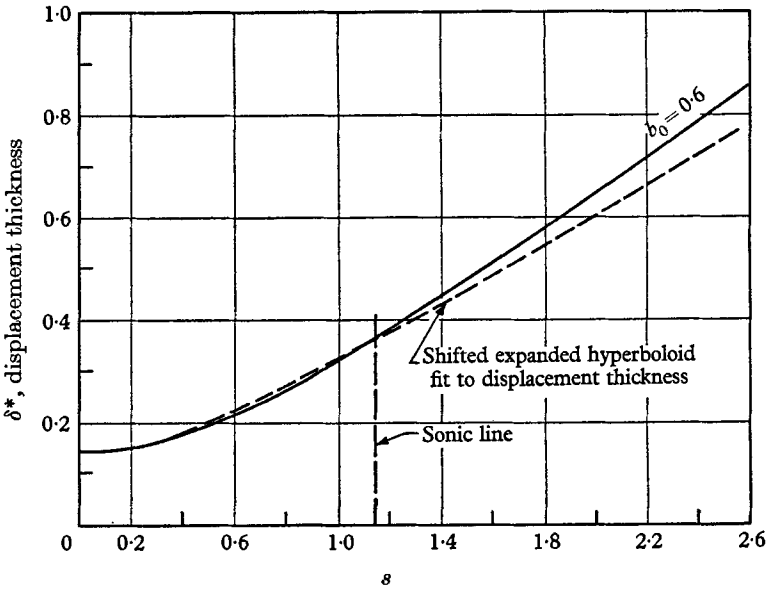

FIGURE 11. Displacement thickness on a hyperboloid at $M_\infty = \infty$, $\gamma = \frac{7}{5}$.

with those for the previous case of flow over a paraboloid with the same free-stream and wall conditions; however, due to the different body shape and pressure distribution these solutions do not agree as well further downstream. The difference between the two cases is never large, and in the case of heat transfer (figure 4) the difference between the two cases is barely distinguishable. If a hyperboloid with steeper asymptotes had been chosen, the difference between the solutions for the paraboloid and hyperboloid would have been larger and differences between the two flow cases would have been more distinguishable.

(*b*) *Second-order solutions for the hyperboloid.* The second-order solutions for the hyperboloid with wall to stagnation-point temperature ratio $b_0 = 0{\cdot}6$ were carried out in exactly the same manner as were those for the paraboloid, and the results are given in figures 12 and 13. The effect of displacement thickness was approximated by shifting and expanding a hyperboloid to fit the original body plus displacement thickness as near as possible. The results of this fit are given in figure 11. The values of the slip and temperature jump constants used are the same as those used in the previous case of the paraboloid.

Most of the second-order results for the hyperboloid are similar to the second-order results for the paraboloid with the notable exceptions of the second-order effects of vorticity interaction and displacement. Figure 12 shows that the

effects of vorticity interaction and displacement on the second-order shear grow with increasing s. These effects will continue to grow as s increases, and eventually the effects of vorticity interaction and displacement will become first-order

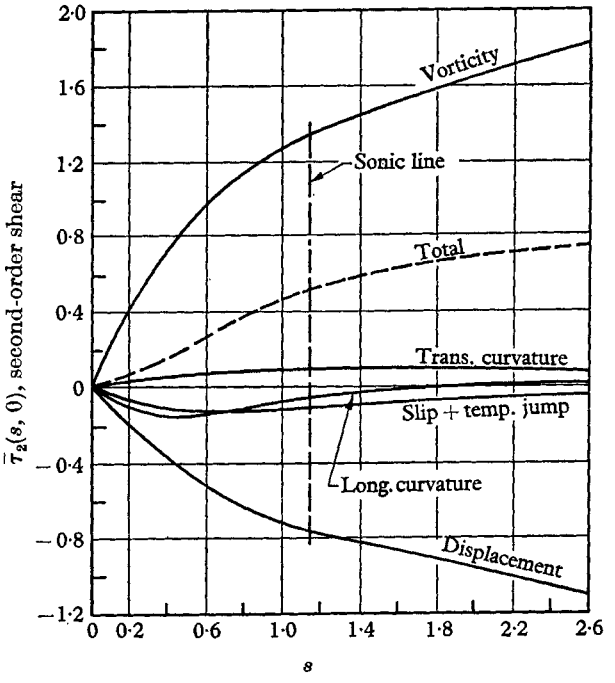

FIGURE 12. Second-order shear on a hyperboloid at $M_\infty = \infty$, $\gamma = \frac{7}{5}$, $b_0 = 0{\cdot}6$.

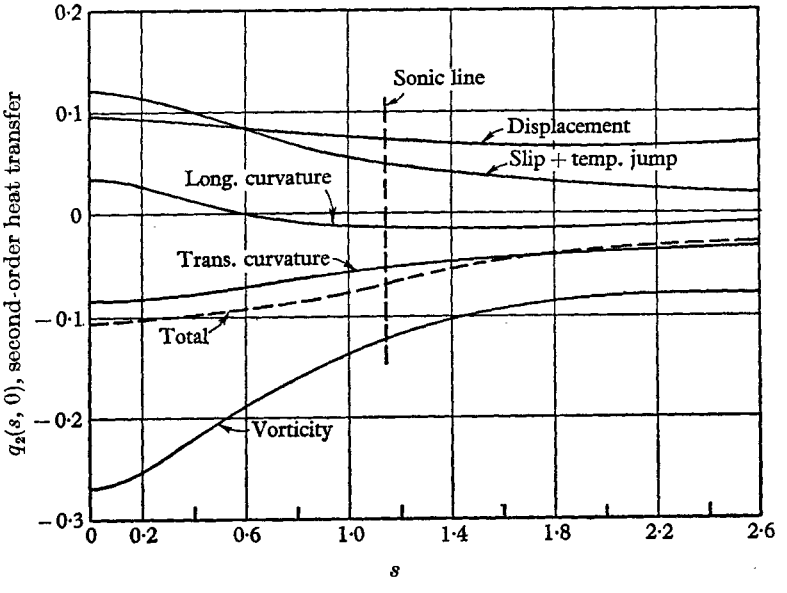

FIGURE 13. Second-order heat transfer on a hyperboloid at $M_\infty = \infty$, $\gamma = \frac{7}{5}$, $b_0 = 0{\cdot}6$.

effects. This can be seen by observing the relation given for the vorticity at the body surface.† This is given by Van Dyke (1962*a*), equation (2.23), as

$$\Omega_1 = r^j(R_1 T_1 S_1')_{n=0} \tag{3.10}$$

or

$$\Omega_1 = \{\gamma/(\gamma-1)\} r^j (P_1 S_1')_{n=0}. \tag{3.11}$$

For the hyperboloid $P_1 \to$ const. (see figure 2) as $s \to \infty$ and $(S_1')_{n=0}$ is a constant for all s. Then the vorticity Ω_1 at the body surface must be proportional to r for the hyperboloid as $s \to \infty$. This means that for large s the effects of vorticity interaction and displacement must become first-order effects. This is the case of strong vorticity interaction which has not been handled so far except for the case of incompressible flow past a flat plate by Ting (1960). The numerical results for the paraboloid (figure 7) do not indicate that this effect of strong vorticity interaction occurs in that case, since the second-order shears at the wall, arising from vorticity and displacement, do not increase after s reaches about 2·0. The case of strong vorticity interaction should be examined in detail by studying the viscous compressible flow past a hyperboloid at a large distance s downstream.

3.5. *Boundary-layer solutions for flow past a sphere at free-stream Mach number* 10·0

The inviscid surface pressure distribution for the flow past a sphere at Mach number 10·0 is given in figure 14. As in the previous cases, this pressure distribution was obtained from a numerical solution to the complete inviscid equations by H. Lomax. The numerical solutions to the boundary-layer equations were carried out in the same manner as in the previous two examples.

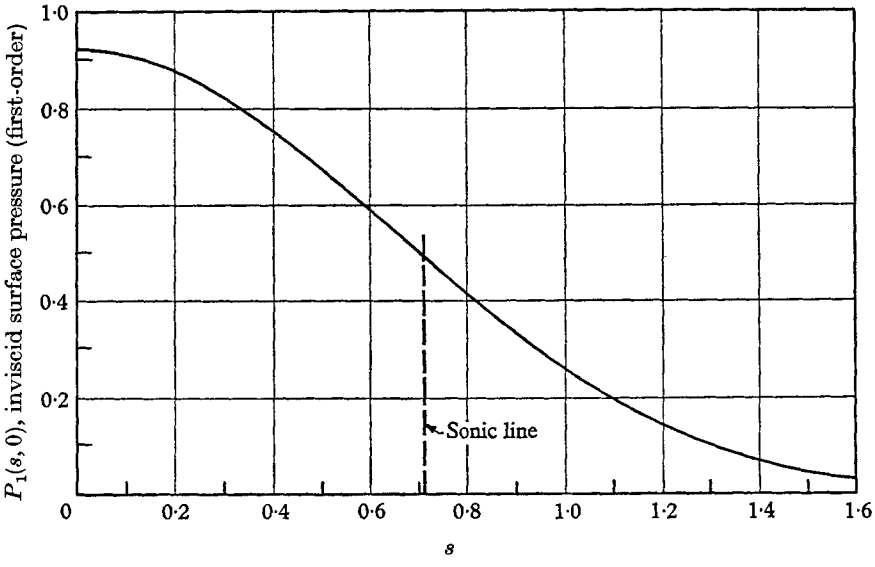

FIGURE 14. Surface-pressure distribution for a sphere at $M_\infty = 10{\cdot}0$, $\gamma = \frac{7}{5}$.

† The manner in which the vorticity enters the effects of vorticity interaction and displacement can be seen from equations (2.18), (2.19), (2.22), and (3.1)–)3.3).

(*a*) *First-order solutions for the sphere.* Figures 15–17 give the first-order results for flow past a sphere at free-stream Mach number 10·0 and with a wall to stagnation-point temperature ratio $b_0 = 0{\cdot}6$. The solutions extend back on

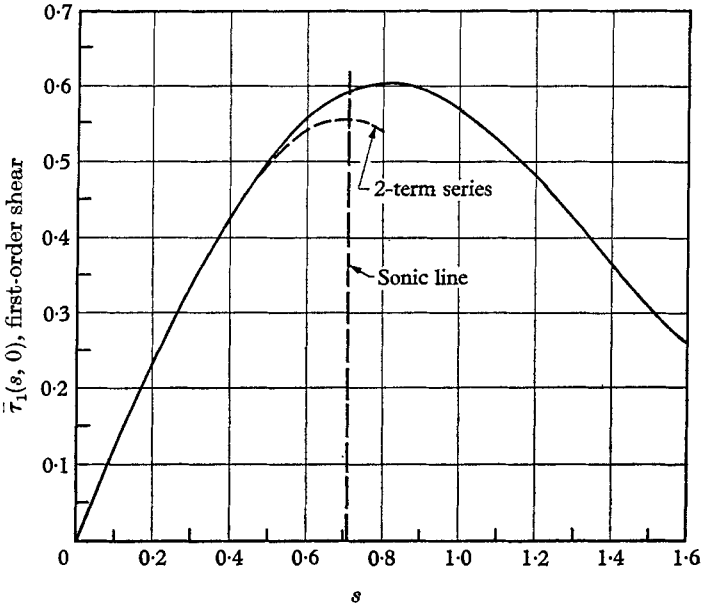

FIGURE 15. First-order shear on a sphere at $M_\infty = 10{\cdot}0$, $\gamma = \frac{7}{5}$, $b_0 = 0{\cdot}6$.

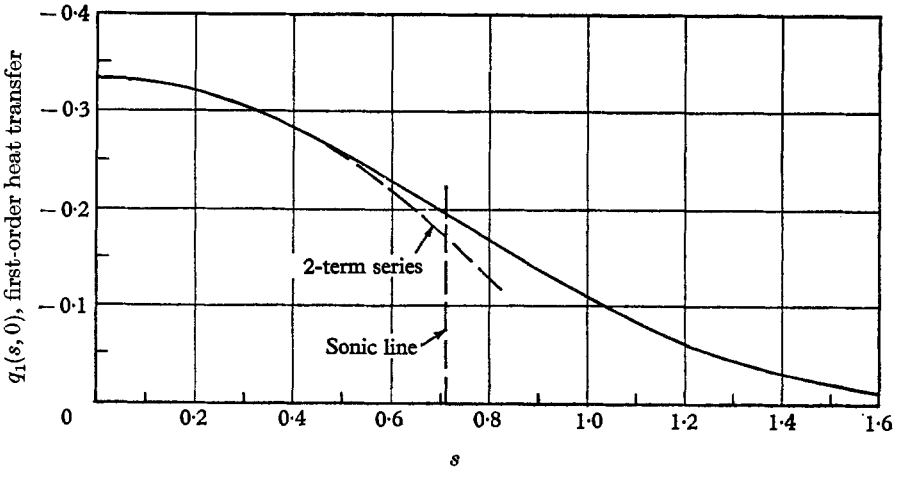

FIGURE 16. First-order heat transfer on a sphere at $M_\infty = 10{\cdot}0$, $\gamma = \frac{7}{5}$, $b_0 = 0{\cdot}6$.

the sphere to $s = 1{\cdot}6$, which is slightly past the mid-point of the sphere. It would be interesting to extend these computations further back to the point of separation; however, the inviscid solution was not available past the point at which the boundary-layer solutions were terminated.

As in the case of flow past a paraboloid, the accuracy of the finite-difference solution was checked by a comparison with two terms of the Blasius series for the

first-order boundary-layer equations for a wall to stagnation-point temperature ratio $b_0 = 0{\cdot}6$. These results can be summarized as in table 2.

As in the case of the paraboloid, the agreement in the finite-difference and series solutions is not so good at first; however, after a few steps in the finite-

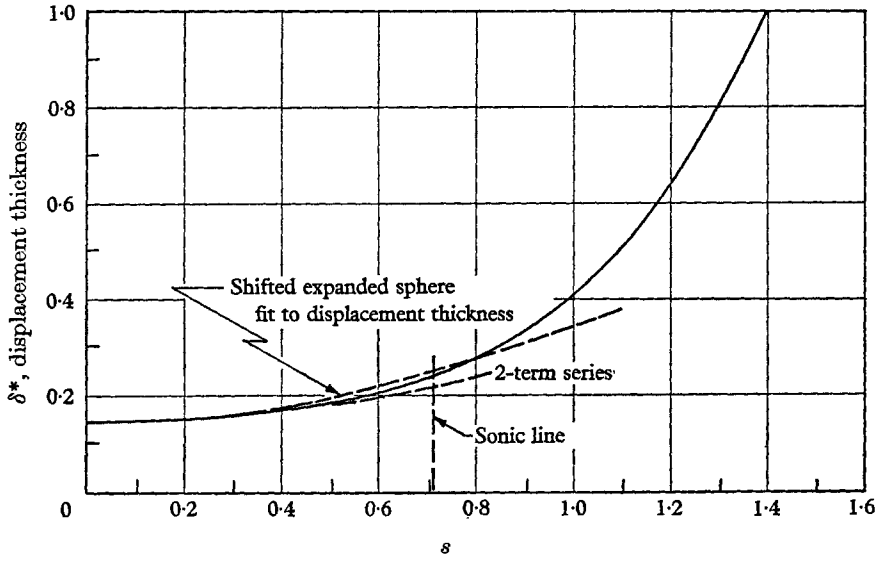

FIGURE 17. Displacement thickness on a sphere at $M_\infty = 10{\cdot}0$, $\gamma = \frac{7}{5}$, $b_0 = 0{\cdot}6$.

	Series results			Finite-difference results		
s	$\bar{\tau}_1(s, 0)$	$q_1(s, 0)$	$\bar{\delta}^*$	$\bar{\tau}_1(s, 0)$	$q_1(s, 0)$	$\bar{\delta}^*$
0·05	0·0593	−0·3358	0·1414	0·0585	−0·3105	0·1373
0·10	0·1179	−0·3334	0·1425	0·1178	−0·3309	0·1422
0·15	0·1754	−0·3293	0·1443	0·1753	−0·3282	0·1442
0·20	0·2310	−0·3255	0·1469	0·2310	−0·3229	0·1469
0·25	0·2843	−0·3162	0·1501	0·2844	−0·3159	0·1503
0·30	0·3345	−0·3072	0·1541	0·3349	−0·3075	0·1546
0·35	0·3812	−0·2965	0·1588	0·3822	−0·2977	0·1598

TABLE 2

difference computations the two solutions agree very well. As s increases more, as before, the finite-difference solutions begin to disagree slightly with the series solution; however, this is due to the limited range of applicability of two terms of the series solution. Figures 15–17 show plots which compare the results of the series solution with the finite-difference solution.

(*b*) *Second-order solutions for the sphere.* Figures 18 and 19 show the second-order results for the shear and heat transfer, respectively, for the sphere. The relations needed in equations (3.1)–(3.3) for computing the second-order effect of displacement thickness are

$$(s_1 - s) = -\epsilon\zeta_1 \sin(s), \tag{3.12}$$

$$(n_1 - n) = -\epsilon[\zeta_2 + \zeta_1\{1 - \cos(s)\}]. \tag{3.13}$$

These were obtained in the same manner as the case for flow past a paraboloid by shifting and expanding the sphere to fit the body given by the original body plus displacement thickness. (See the parabola example for the definition of ζ_1 and ζ_2.) The accuracy of this fit is shown in figure 17. The fit is good up to about $s = 0{\cdot}9$ but is poor thereafter. This will affect the results for the second-order effect of displacement thickness in figures 18 and 19 for $s > 0{\cdot}9$.

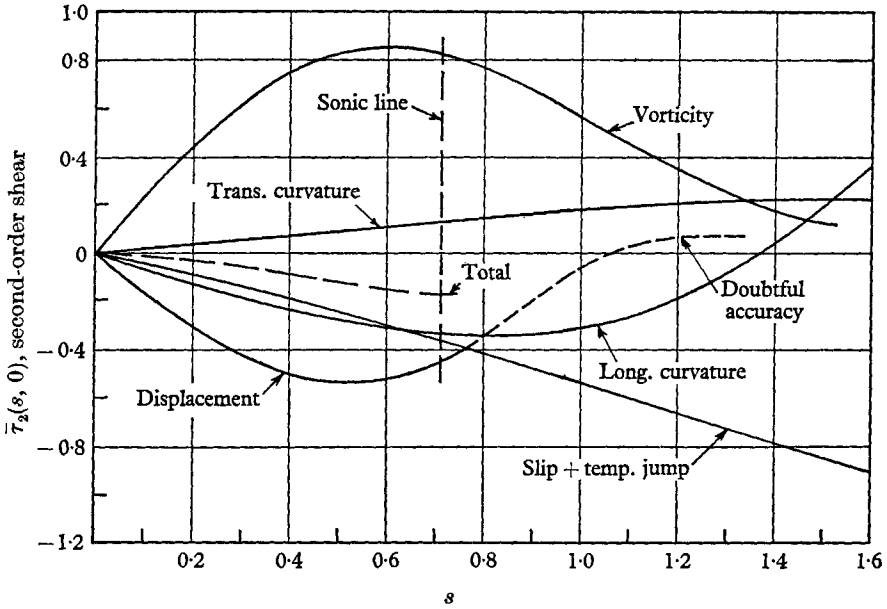

FIGURE 18. Second-order shear on a sphere at $M_\infty = 10{\cdot}0$, $\gamma = \frac{7}{5}$, $b_0 = 0{\cdot}6$.

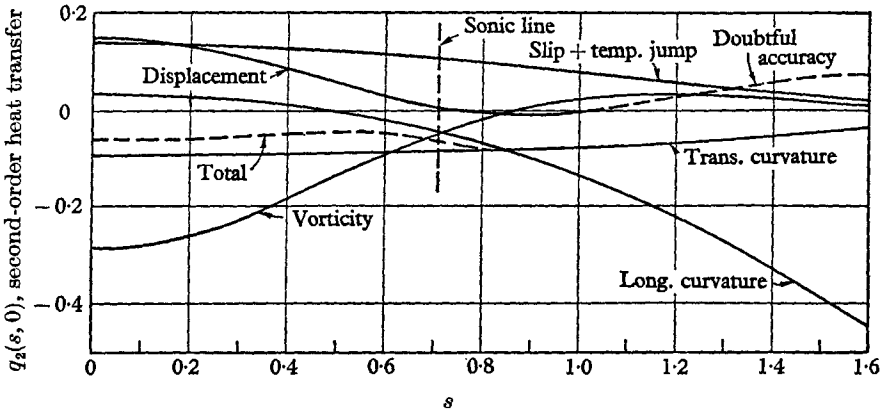

FIGURE 19. Second-order heat transfer on a sphere at $M_\infty = 10{\cdot}0$, $\gamma = \frac{7}{5}$, $b_0 = 0{\cdot}6$.

One interesting aspect for flow past the sphere is the behaviour of the second-order terms far downstream. It is well known that first-order boundary-layer theory is not valid in the reversed flow region after separation. As in other perturbation problems, one expects then that in approaching this region where the expansion is not valid, the solution of the second-order boundary-layer equations will indicate this invalidity. The computations here have not been

carried as near separation as one would hope for in examining this point; however, the effect of longitudinal curvature, for example on the shear in figure 18, seems to indicate that this effect is becoming very large as separation is approached. In order to examine another quantity of interest near separation, we have plotted v_1 and v_2 (first- and second-order velocity components normal to the body surface) at a representative value of $N = 1{\cdot}3722$ in figure 20. This figure clearly indicates that the v_2 component due to longitudinal curvature is becoming very large near separation. The other second-order terms do not demonstrate as drastic a behaviour near separation as far as can be determined from the numerical results. This indicates that this v_2 component near separation is no longer a second-order quantity and therefore that the boundary-layer expansion (equations (2.6*a–f*)) is not valid in the region of separation. This is what one would expect; however, this has not been exhibited in this manner until now.

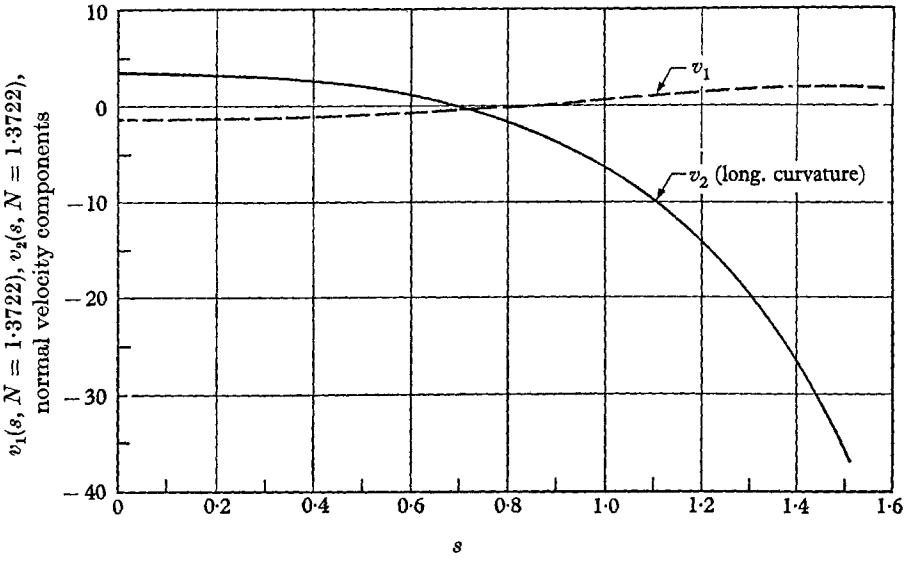

FIGURE 20. First- and second-order normal velocity components at $N = 1{\cdot}3722$ on a sphere at $M_\infty = 10{\cdot}0$, $\gamma = \frac{7}{5}$, $b_0 = 0{\cdot}6$.

3.6. *Comparison with other theories and experiments*

Kinslow & Potter (1962) have performed drag experiments on spheres for high Mach number flows at low Reynolds numbers.† These results are presented by them for a variety of free-stream and wall conditions. The drag on the spheres is made up of two parts, one part due to the pressure and another part due to the shear at the surface of the sphere. In terms of a drag coefficient this can be expressed as

$$C_D = 4\int_0^\pi p(s,0)\, r\cos s\, ds + 4\int_0^\pi \bar{\tau}(s,0)\, r\sin s\, ds, \tag{3.14}$$

where

$$C_D = D/\tfrac{1}{2}\pi a^{*2}\rho_\infty^* U_\infty^{*2} \tag{3.15}$$

is the drag coefficient and D is the total drag.

† The range of the values of the Reynolds number Re_s in their experiments was from about 1 to 6000.

In the boundary-layer region prior to separation, $p(s,0)$ and $\bar{\tau}(s,0)$ can be expressed as (see equations (2.6*c*) and (2.28))

$$p(s,0) = p_1(s,0) + \epsilon p_2(s,0) + \epsilon^2 p_3(s,0) + \ldots, \tag{3.16}$$

$$\bar{\tau}(s,0) = \epsilon \bar{\tau}_1(s,0) + \epsilon^2 \bar{\tau}_2(s,0) + \ldots. \tag{3.17}$$

At high free-stream Mach numbers the contribution to the drag due to back pressure on the spheres should be small and will therefore be neglected. The contribution to drag due to shear in the region beyond separation should also be small and will also be neglected. Doing this we can get a good approximation to the sphere drag using only boundary-layer theory.

Kinslow & Potter (1962) have fitted curves to their results to include terms of order ϵ^2 in the drag coefficient. It is possible to compute from equation (3.14) the contribution to drag due to shear to order ϵ^2 from equation (3.17); however, we cannot compute the pressure part to that order since $p_3(s,0)$ is not known in equation (3.16) and would involve solving the outer flow problem to third-order. This would prove difficult since viscous terms in the outer flow enter in the third-order terms, and it is not possible to approximate the flow by a shifted, expanded body, as was done in the second-order case. For this reason we are able to compare only the sphere drag to order ϵ with Kinslow & Potter (1962).

For particular cases we take spheres at free-stream Mach number 10 with wall to stagnation-point temperature ratios b_0 of 0·2 and 0·6. The quantity $p_1(s,0)$ is obtained from the numerical results provided by Lomax. $p_2(s,0)$ is given by Van Dyke (1962*a*), equation (2.46), as

$$p_2(s,0) = \kappa \int_0^\infty \{R_1(s,0)\, U_1^2(s,0) - \rho_1 u_1^2\}\, dN + P_2(s,0), \tag{3.18}$$

where $P_2(s,0)$ is computed in the same manner as $U_2(s,0)$, etc., in equations (3.1)–(3.3) by shifting and expanding the sphere to fit the body plus displacement thickness. The integral on the right-hand side of equation (3.18) is evaluated numerically.

The sphere-drag computation is carried out numerically by using Simpson's rule on equation (3.14). The integrands appearing in equation (3.14) are obtained from the finite-difference solution. For the case of wall to stagnation-point temperature ratio $b_0 = 0{\cdot}2$, the results are

$$C_D = 0{\cdot}89 + 1{\cdot}7\epsilon, \tag{3.19}$$

and, for $b_0 = 0{\cdot}6$,

$$C_D = 0{\cdot}89 + 2{\cdot}3\epsilon. \tag{3.20}$$

Converting ϵ to the Reynolds number based on conditions behind the shock used by Kinslow & Potter (1962), we obtain

$$C_D = 0{\cdot}89 + 2{\cdot}8/Re_s^{\frac{1}{2}} \tag{3.21}$$

for $b_0 = 0{\cdot}2$, and

$$C_D = 0{\cdot}89 + 3{\cdot}8/Re_s^{\frac{1}{2}} \tag{3.22}$$

for $b_0 = 0{\cdot}6$. Re_s is a Reynolds number defined as

$$Re_s = U_s^* \rho_s^* D^* / \mu_s^*, \tag{3.23}$$

where U_s^*, ρ_s^* and μ_s^* are the velocity, density and viscosity, respectively, behind the shock, and D^* is the body nose diameter.

Using this definition of Re_s, the definition of ϵ, and some thermodynamic relations, we find that

$$\epsilon = \sqrt{2}\left[\frac{(\gamma-1)(\gamma+1)^2 M_\infty^4}{[2\gamma M_\infty^2-(\gamma-1)][(\gamma-1)M_\infty^2+2]}\right]^{\frac{1}{2}\omega}\frac{1}{\sqrt{Re_s}}. \tag{3.24}$$

The first result for $b_0 = 0{\cdot}2$ compares favourably with the value of

$$C_D = 0{\cdot}92 + 2{\cdot}1/Re_s^{\frac{1}{2}} \tag{3.25}$$

obtained by Kinslow & Potter (1962) for their case of $b_0 = 0{\cdot}15$. The slightly larger coefficient which we obtained in the second term is due, at least in part, to the colder wall in the Kinslow & Potter experiments. It is not possible to compare the case of $b_0 = 0{\cdot}6$ with any of the experimental results of Kinslow & Potter (1962); however, an examination of their results does show that it is at least the right order of magnitude.†

Cheng (1963) has developed a method for computing the viscous flow past blunt bodies in hypersonic flow. He has computed several examples, one of which is the case of flow past a paraboloid with wall to stagnation-point temperature ratio $b_0 = \frac{1}{8}$. If the results for heat transfer and skin friction of this case are compared with the case computed here for $b_0 = 0{\cdot}2$ (see figures 9 and 10), it is found that the agreement between the two methods is good for ϵ small if one considers only first-order boundary-layer theory. (This corresponds to large values of K^2 in Cheng's method.) If one adds the second-order contributions from figures 19 and 20, then the comparison is not as good. This is understandable since, as mentioned in § 2, Cheng has not included most of the second-order effects in his analysis.

This research was supported by the Air Force Office of Scientific Research, Office of Aerospace Research under Grants AF-AFOSR-62-242 and AF-AFOSR-235-63.

REFERENCES

BAXTER, D. C. & FLÜGGE-LOTZ, I. 1957 The solution of compressible laminar boundary layer problems by a finite-difference method, Part II. Further discussion of the method and computation of examples. *Div. Engng Mech., Stanford Univ., Tech. Rep.* no. 110. (Abbreviated version published in *Z. angew. Math. Phys.* **9b**, 81–96.)

CHAPMAN, S. & COWLING, T. G. 1961 *The Mathematical Theory of Non-Uniform Gases.* Cambridge University Press.

CHENG, H. K. 1963 The blunt-body problem in hypersonic flow at low Reynolds number. *Cornell Aero. Lab. Rep.* no. AF-1285-A-10.

DAVIS, R. T. & FLÜGGE-LOTZ, I. 1963 Laminar compressible flow past axisymmetric blunt bodies (results of a second-order theory). *Div. Engng Mech., Stanford Univ., Tech. Rep.* no. 143.

DAVIS, R. T. & FLÜGGE-LOTZ, I. 1964 The laminar compressible boundary-layer in the stagnation-point region of an axisymmetric blunt body including the second-order effect of vorticity interaction. *Int. J. Heat & Mass Transf.* **7**, 341–70.

ERDELYI, A. 1961 An expansion procedure for singular perturbations. *Atti della Scienze de Torino*, **95**.

† Even though the third term in the series for C_D has not been computed here, one can see from figure 18 that if the contribution due to pressure is neglected, the third term should have a negative sign. This is in agreement with the experiments of Kinslow & Potter (1962).

FLÜGGE-LOTZ, I. & BAXTER, D. C. 1956 The solution of compressible laminar boundary layer problems by a finite difference method. *Div. Engng Mech., Stanford Univ., Tech. Rep.* no. 103.

FLÜGGE-LOTZ, I. & BLOTTNER, F. G. 1962 Computation of the compressible laminar boundary-layer flow including displacement-thickness interaction using finite-difference methods. *Div. Engng Mech., Stanford Univ., Tech Rep.* no. 131. (Abbreviated version published in *J. Méchanique*, **2**, 397–423.)

FLÜGGE-LOTZ, I. & YU, E. Y. 1960 Development of a finite-difference method for computing a compressible laminar boundary-layer with interaction. *Div. Engng Mech., Stanford Univ., Tech. Rep.* no. 127 (*AFOSR TN* 60–577).

INOUYE, M. & LOMAX, H. 1962 Comparison of experimental and numerical results for the flow of a perfect gas about blunt-nosed bodies. *NASA Tech. Note* no. D-1426.

KINSLOW, M. & POTTER, J. L. 1962 The drag of spheres in rarefied hypervelocity flow. *Arnold Engng Devt. Center, Tech. Rep.* no. AEDC-TDR-62-205 (also in *AIAA J.* **1**, 2467–2473).

LAGERSTROM, P. A. 1957 Note on the preceding two papers. *J. Math. Mech.* **6**, 605.

LENARD, M. 1962 Stagnation point flow of a variable property fluid at low Reynolds numbers. Cornell University Thesis.

MASLEN, S. H. 1958 On heat transfer in slip flow. *J. Aero Sci.* **25**, 400.

MASLEN, S. H. 1962 Second order effects in laminar boundary layers. *Martin Co. Res. Rep. PR*-29 (also in *AIAA J.* **1**, 33–40).

PETROVSKY, I. G. 1954 *Lectures on Partial Differential Equations.* New York: Interscience.

PROBSTEIN, R. F. 1961 Shock-wave and flow field development in hypersonic re-entry. *ARS J.* **31**, 185.

RAETZ, G. S. 1957 A method of calculating three-dimensional laminar boundary layers of steady compressible flows. *Northrop Aircraft, Inc., Rep.* no. NAI-58-73.

SMITH, A. M. O. & CLUTTER, D. W. 1963*a* Solution of the incompressible laminar boundary-layer equations. *AIAA J.* **1**, 2062–2071.

SMITH, A. M. O. & CLUTTER, D. W. 1963*b* Solution of Prandtl's boundary-layer equations. *Douglas Aircraft Company Engng Paper* 1530.

STREET, R. E. 1960 A study of boundary conditions in slip-flow aerodynamics. *Rarefied Gas Dynamics* (ed. F. M. Devienne), pp. 276–92. London: Pergamon Press.

TING, L. 1960 Boundary layer over a flat plate in presence of shear flow. *Phys. Fluids*, **3**, 78.

VAN DYKE, M. 1962*a* Second-order compressible boundary-layer theory with application to blunt bodies in hypersonic flow. *Hypersonic Flow Research* (ed. F. R. Riddell), pp. 37–76. New York: Academic Press.

VAN DYKE, M. 1962*b* Higher approximations in boundary-layer theory. Part 1. *J. Fluid Mech.* **14**, 161.

WU, J. C. 1960 The solution of laminar boundary-layer equations by the finite difference method. *Douglas Aircraft Company, Inc., Rep.* no. SM-37484 (see also, On the finite difference solution of laminar boundary layer problems, in *Proc.* 1961 *Heat Trans. & Fluid Mech. Inst.*, Stanford Univ. Press).